# Image Segmentation for Intensity Inhomogeneity in Presence of High Noise

**Article** *in* IEEE Transactions on Image Processing · April 2018

DOI: 10.1109/TIP.2018.2825101

CITATIONS
2

READS
173

**3 authors:**

Haider Ali
University of Peshawar
**10** PUBLICATIONS **60** CITATIONS
SEE PROFILE

Lavdie Rada
Bahçeşehir University
**13** PUBLICATIONS **140** CITATIONS
SEE PROFILE

Noor Badshah
University of Engineering and Technology, Peshawar
**40** PUBLICATIONS **245** CITATIONS
SEE PROFILE

# Image Segmentation for Intensity Inhomogeneity in Presence of High Noise

Haider Ali, Lavdie Rada, and Noor Badshah

***Abstract*— Automated segmentation of fine objects details in a given image is becoming of crucial interest in different imaging fields. In this paper, we propose a new variational level-set model for both global and interactive\selective segmentation tasks, which can deal with intensity inhomogeneity and the presence of noise. The proposed method maintains the same performance on clean and noisy vector-valued images. The model utilizes a combination of locally computed denoising constrained surface and a denoising fidelity term to ensure a fine segmentation of local and global features of a given image. A two-phase level-set formulation has been extended to a multi-phase formulation to successfully segment medical images of the human brain. Comparative experiments with state-of-the-art models show the advantages of the proposed method.**

***Index Terms*— Image segmentation, selective segmentation, interactive segmentation, calculus of variations, level set method, partial differential equations, multi-phase formulation.**

## I. Introduction

VARIOUS models for image segmentation have been extensively studied and successfully implemented in image analysis, pattern recognition, image understanding, computer vision, etc. There are two different segmentation classes: 1) global segmentation, where the contour of all the objects in a given image is required to be segmented, and 2) interactive\ selective segmentation where the task of segmentation is to segment a particular object\ feature of the given image.

The existing global segmentation models can be classified as unsupervised and supervised methods. Three are the main categories for the unsupervised segmentation: edge-based models [14], [16], [29], statistical-based models [1], [9], [15], [18], [31], [34] and mixed models [5]–[7]. Edge based models employ image gradient information and edge detector functions to attract the dynamic contours toward the boundaries of objects. This category may not produce desirable results for noisy images, as it uses image gradient information [5], [18] for segmentation. On the other hand, region-based models do not require image gradient information. Those models use the image statistical information which show better results in presence of noise than edge-based models [9], [34], but it may work poorly with clusters with different densities and sizes [15]. Mixed models combines image gradients and image region statistical information [5]–[7] for a better segmentation accuracy and robustness. The region information acts globally, whereas image gradient information acts locally to identify the edges. On the other hand, supervised segmentation techniques has been broadly investigated in the last decades in machine learning and pattern recognition. Deep learning algorithms, in particular convolutional networks [4], [8], [10], [17], [19], have rapidly become an automated methodology of analyzing different classes in a given image. However, *a*) their large training sets makes them limited by the lack of generalization to previously unseen object classes, *b*) can not demonstrated sufficient accuracy for images with poor quality and intensity inhomogeneity [35], *c*) or demonstrates good accuracy for inhomogeneous images for a certain given class and the outputs are categories such as cancer or non-cancer [28].

Images with intensity inhomogeneity with or without noise are a challenge for all the global segmenting models. An early attempt to segment images with intensity inhomogeneity was an extension of the 2-phase Chan-Vese (CV) model [9] to a multi-phase model [1], where several level set functions were employed to increase the number of regions of distinct objects. The drawback of the multi-phase model for objects with intensity inhomogeneity is that one object can be segmented by different level sets and recognized as two different objects. To improve the performance of the multiphase CV model, several research have been introduced in the recent years. For example, Li *et al.* [18] proposed the local binary fitting (LBF) model and its multi-phase version, which utilizes local image information by employing a Gaussian kernel function. Although LBF is an improvement over the CV model in cases of image inhomogeneity, the model is not designed for noisy images. The local image fitting (LIF) model, proposed by Zhang *et al.* [34], is similar and utilizes local image information to improve segmentation of images with intensity inhomogeneity. Wang *et al.* [31] introduced additional constraints combined with CV model, which we shortly will refer as local CV (LCV) model. They used the intensity averages of the difference of the given image with averaging convoluted image to get more local information and segment better intensity inhomogeneity images. More recently, Akram *et al.* [2] introduced a model using a concept of

Manuscript received August 10, 2017; revised January 26, 2018 and March 23, 2018; accepted March 27, 2018. Date of publication April 19, 2018; date of current version April 26, 2018. The associate editor coordinating the review of this manuscript and approving it for publication was Prof. Peter Tay. *(Corresponding author: Lavdie Rada.)*

H. Ali is with the Department of Mathematics, University of Peshawar, Peshawar 25120, Pakistan (e-mail: dr.haider@uop.edu.pk).

L. Rada is with the Department of Biomedical Engineering, Bahçeşehir University, 34349 Istanbul, Turkey (e-mail: lavdie.rada@eng.bau.edu.tr).

N. Badshah is with the Department of Basic Sciences, University of Engineering and Technology at Peshawar, Peshawar 25120, Pakistan (e-mail: noor2knoor@gmail.com).

Color versions of one or more of the figures in this paper are available online at http://ieeexplore.ieee.org.

Digital Object Identifier 10.1109/TIP.2018.2825101

difference image embedded in signed pressure force function (spf). The model uses the difference image as a subtraction of the local fitted image used in LIF model [34]. In a different approach, Wu and He [33] overcome the drawbacks of the CV model by utilizing a new data fidelity term based on the concept of the coefficient of variation as an edge detector [6]. Even though the above mentioned models perform better than old models, the performance is still significantly affected by noise and inhomogeneity. Additionally, to the best of our knowledge there is no machine learning technique that can deal with general case of inhomogenity image segmentation.

In many segmentation problems, we only need to segment a particular object of interest rather than all boundaries in the image. This is a task of interactive\ selective segmentation, in which a target object is detected. This type of segmentation is relatively new. An edge-based method for selective segmentation was introduced in the work of [5], [15], and [23]. Two other methods, random walks [13], graph cut [25], use the probability distributions or graph cut theory respectively, to improve over the old models. In the work of Nguyen *et al.* [21], geometric points outside and inside the objects direct the continuous-domain convex active contours for a successful interactive segmentation computing previous methods such as [25] and [30]. Recently, in the work of Rada and Chen [24] an interactive variational model has been introduced. The model improves the old variational models [5], [14] and competes the state of art introduced by Nguyen *et al.* [21]. However, selective segmentation models mentioned above are not designed to cope with images containing intensity inhomogeneity.

In this paper we propose a new variational region-based active contour model for both tasks of segmentation, global and selective, for intensity inhomogeneity images with or without noise. To handle high image noise we employ two data fidelity terms. To improve the old segmentation models we employ local image information in both the data fidelity terms and get profit from denoising terms which balance trade-off between additive and multiplicative noise. In this way the model can easily handle image intensity inhomogeneity and show capability to distinguish meaningful feature from tiny noisy detail. First, we introduce a two-phase level set formulation, which is extended to a multi-phase formulation, to successfully segment medical brain images with and without noise. We fit the same idea for the selective segmentation task by improving over old models, such as over Rada and Chen [24]. The rest of the paper is organized as follows. Setion 2, reviews some classical models and indicates their limitations. Section 3 describes the variational formulation of our models in global and selective segmentation tasks. Section 4, presents the experimental results. Section 5 concludes our work with a discussion and future directions.

## II. Background

Image denoising and image segmentation are the fundamental tasks in image processing. The aim in a denoising process is to recover a clean image $z(\mathbf{x})$, given a noisy image $z_0(\mathbf{x})$, where $z(\mathbf{x})$ and $z_0(\mathbf{x})$ are given functions in a bounded open subset $\Omega$, $z(\mathbf{x}) : \Omega \longrightarrow \mathbf{R}$ and $z_0(\mathbf{x}) : \Omega \longrightarrow \mathbf{R}$, respectively. There are two different types of noise that should be distinguish: additive and multiplicative noise. Most studies deal with the additive noise model, in which the clean image $z(\mathbf{x})$ has been corrupted by some additive noise $\eta(\mathbf{x})$, giving the data $z_0(\mathbf{x}) = z(\mathbf{x}) + \eta(\mathbf{x})$. In particular, we can mention the famous classical variational denoising model introduced by Rudin-Osher-Fatemi (ROF) [26], which proposed the following energy functional:

$$F^{ROF}(z(\mathbf{x})) = \int_\Omega |\nabla z(\mathbf{x})| d\mathbf{x} + \lambda \int_\Omega \Big(z(\mathbf{x}) - z_0(\mathbf{x})\Big)^2 d\mathbf{x}. \quad (1)$$

In this function the first term keeps the smoothness of the image to be reconstructed, while the second term deals with the fit between the reconstructed image and the given image. This model, and other similar works dealing with additive noise [11], [12], [22], may not work properly when an image is corrupted with multiplicative noise.

For the case of multiplicative noise, to recover a clean image $z(\mathbf{x})$ from the given data $z_0(\mathbf{x}) = z(\mathbf{x})\eta(\mathbf{x})$, where $z_0(\mathbf{x})$ is an observed image corrupted by some multiplicative noise $\eta(\mathbf{x})$, Aubert and Aujol [3] showed successful numerically results of the following functional for the multiplicative denoising problem:

$$F^{AA}(z(\mathbf{x})) = \int_\Omega |\nabla z(\mathbf{x})| d\mathbf{x} + \lambda \int_\Omega \Big(\log(z(\mathbf{x})) + \frac{z_0(\mathbf{x})}{z(\mathbf{x})}\Big) d\mathbf{x}. \quad (2)$$

The AA model competes with all the previous denoising models.

On the other hand, in contrast with denoising, the aim of the image segmentation process is to divide a given image $z_0(\mathbf{x})$ into regions with a contour $\Gamma$, each of which represents a meaningful object. One of the well-known segmentation models is the CV model [9]. The CV model considers the image as a piecewise constant function with value $c_1$ and $c_2$ in the foreground ($in(\Gamma)$), and background ($out(\Gamma)$), respectively. To solve the inverse problem, they proposed the minimization of the following energy functional:

$$F^{CV}(c_1, c_2, \Gamma) = \mu \ \text{length}(\Gamma) + \lambda_1 \int_{in(\Gamma)} |z_0(\mathbf{x}) - c_1|^2 d\mathbf{x} + \lambda_2 \int_{out(\Gamma)} |z_0(\mathbf{x}) - c_2|^2 d\mathbf{x}, \quad (3)$$

where $\Gamma$ is the boundary of the segmented objects, $c_1$ and $c_2$ are the average intensities inside and outside $\Gamma$), respectively. $\mu \geq 0$, $\lambda_1 > 0$, $\lambda_2 > 0$ are fixed parameters, such as $\mu$ controls the size of objects and $\lambda_1, \lambda_2$ control the image data driven force inside and outside the contours, respectively.

To solve the above minimization problem a level set function $\phi(\mathbf{x})$ has been introduced [22], [27],

$$\begin{cases} \Gamma = \{(\mathbf{x}) \in \Omega : \phi(\mathbf{x}) = 0\}, \\ in(\Gamma) = \{(\mathbf{x}) \in \Omega : \phi(\mathbf{x}) > 0\}, \\ out(\Gamma) = \{(\mathbf{x}) \in \Omega : \phi(\mathbf{x}) < 0\}, \end{cases} \quad (4)$$

and the Eq. (3) is rewritten as:

$$F^{CV}(c_1, c_2, \Gamma) = \mu \int |\nabla H_\epsilon(\phi)| d\mathbf{x} + \lambda_1 \int |z_0(\mathbf{x}) - c_1|^2 H_\epsilon(\phi) d\mathbf{x} + \lambda_2 \int |z_0(\mathbf{x}) - c_2|^2 (1 - H_\epsilon(\phi)) d\mathbf{x}$$

where $H_\epsilon(\phi)$ is the differentiable versions of the Heaviside function. For our experimental tests we used the following $H_\epsilon(\phi)$ and its corresponding Delta function $\delta_\epsilon(\phi)$:

$$H_\epsilon(z) = \frac{1}{2}\Big(1 + \frac{2}{\pi}\arctan(\frac{z}{\epsilon})\Big), \quad \delta_\epsilon(z) = \frac{\epsilon}{\pi\left(\epsilon^2 + z^2\right)}.$$

The equation is completely managed across the boundary by the mean curvature and the jump of the data energy term. Although the CV model is non-convex, it has been widely used and has successfully solved many practical problems, as long as the image intensities are close to the piecewise constant. However, beyond its original assumption, extending the CV model to segment images containing objects with inhomogeneous intensities has been the subject of several recent works [6], [7], [31]. To improve the CV model for images with intensity inhomogeneity, Wu and He [33] proposed a coefficient of variation based model (CVM) with a strictly convex energy functional in a level set formulation of the form:

$$E^{CVM}(\phi, c_1, c_2) = \mu \int_\Omega \frac{(z(\mathbf{x}) - c_1)^2}{c_1^2}(\phi(\mathbf{x}) + 1)^2 d\mathbf{x} + \int_\Omega \frac{(z(\mathbf{x}) - c_2)^2}{c_2^2}(\phi(\mathbf{x}) - 1)^2 d\mathbf{x}, \quad (5)$$

where $\mu$, $c_1$ and $c_2$ are constants.

Wang *et al.* [31] introduced a local statistical fitting model. The energy functional in level set formulation is given by:

$$\begin{aligned} &F_\epsilon^{LCV}(\phi, c_1, c_2, d_1, d_2) \\ &= \mu \int_\Omega \delta_\epsilon(\phi)|\nabla\phi| d\mathbf{x} \\ &\quad + \int_\Omega \frac{1}{2}(|\nabla\phi| - 1)^2 d\mathbf{x} + \lambda_1 \int_\Omega (z_0 - c_1)^2 H_\epsilon(\phi) d\mathbf{x} \\ &\quad + \lambda_1 \int_\Omega (z_0 - c_2)^2 (1 - H_\epsilon(\phi)) d\mathbf{x} + \lambda_2 \int_\Omega (z_0^* - z_0 - d_1)^2 H_\epsilon(\phi) d\mathbf{x} \\ &\quad + \lambda_2 \int_\Omega (z_0^* - z_0 - d_2)^2 (1 - H_\epsilon(\phi)) d\mathbf{x}, \end{aligned}$$

where $\mu$, $\lambda_1$, $\lambda_2$ are constants and are used for assigning different weights, similar to CV model, and $z_0^*(\mathbf{x}) = g_k * z_0(\mathbf{x})$ is the convolution of the given image with a averaging convolution operator $g_k$ with window size $k \times k$. In contrast with the CV model, the local image data functional in the LCV model helps to better capture fine details and to detect objects/regions with intensity inhomogeneity [31]. However, for images with high level noise, the LCV model may have to compromise between retaining noise as objects and keeping valuable fine details. That is, either the LCV model avoids noise but misses important detail or it may capture fine detail, but unfortunately, some noise as well. This phenomena can be witnessed in Fig. 1.

Li *et al.* [18] proposed a local binary fit (LBF) which deals with intensity inhomogeneity of the images. The model utilizes a kernel function to enhance the CV model. The fitting energy term of the model is given as follows:

$$\begin{aligned} &F^{LBF}(c, f_1, f_2) \\ &= \lambda_1 \int \kappa_\sigma(\mathbf{x} - \mathbf{y})|z_0(\mathbf{y}) - f_1(\mathbf{x})|^2 H(\phi(\mathbf{y})) d\mathbf{y} \\ &\quad + \lambda_2 \int \kappa_\sigma(\mathbf{x} - \mathbf{y})|z_0(\mathbf{y}) - f_2(\mathbf{x})|^2 (1 - H(\phi(\mathbf{x}))) d\mathbf{y}, \end{aligned} \quad (6)$$

where $\kappa_\sigma(\mathbf{x})$ is a Gaussian Kernel of the form $\kappa_\sigma(\mathbf{x}) = \frac{1}{(2\pi)^{n/2}\sigma^2}.e^{-|\mathbf{x}|^2/2\sigma^2}$, with a scale parameter $\sigma > 0$. It should be emphasized that the functions $f_1(\mathbf{x})$ and $f_2(\mathbf{x})$, which minimize the energy (6), vary with the center point $\mathbf{x}$, which makes the LBF model essentially different from the CV model. Minimizing Eq. (6) respect $f_1(\mathbf{x})$ and $f_2(\mathbf{x})$ we have as follows:

$$\begin{aligned} f_1(x) &= \frac{\kappa_\sigma(x) * H_\varepsilon(\phi(x)) u_0(x)}{\kappa_\sigma(x) * H_\varepsilon(\phi(x))}, \\ f_2(x) &= \frac{\kappa_\sigma(x) * (1 - H_\varepsilon(\phi(x))) u_0(x)}{\kappa_\sigma(x) * (1 - H_\varepsilon(\phi(x)))}. \end{aligned} \quad (7)$$

Keeping $f_1(\mathbf{x})$ and $f_2(\mathbf{x})$ fixed and minimizing the above energy functional with respect to $\phi$, we get the following equation,

$$\frac{\partial\phi}{\partial t} = \mu(\nabla^2\phi - div(\frac{\nabla\phi}{\nabla\phi})) - \delta_\epsilon(\phi)\left\{(\lambda_1 e_1 - \lambda_2 e_2) + \nu div(\frac{\nabla\phi}{|\nabla\phi|})\right\} \quad (8)$$

where $e_1$ and $e_2$ are given by:

$$\begin{aligned} e_1(\mathbf{x}) &= \int_\Omega \kappa_\sigma(\mathbf{x} - \mathbf{y})|z_0(\mathbf{x}) - f_1|^2 d\mathbf{y} \\ e_2(\mathbf{x}) &= \int_\Omega \kappa_\sigma(\mathbf{x} - \mathbf{y})|z_0(\mathbf{x}) - f_2|^2 d\mathbf{y}. \end{aligned}$$

Even though, we clearly can see that the fitting term empowers LBF model by providing accurate segmentation results in the presence of intensity inhomogeneity, the model struggles in presence of noise, as shown in the second row of Fig. 2 2a and 2b. To segment images with intensity inhomogeneity, Zhang *et al.* [34] proposed a local image fitting energy functional by minimizing the difference between the fitted image and the original image. The formulation is as follows:

$$E^{LIF}(\phi) = \frac{1}{2}\int_\Omega |z_0(\mathbf{x}) - z'(\mathbf{x})|^2 d\mathbf{x}, \quad (9)$$

where $z'(\mathbf{x})$ represents a locally computed image (LCI) as follows:

$$z'(\mathbf{x}) = m_1 H_\epsilon(\phi(\mathbf{x})) + m_2\Big(1 - H_\epsilon(\phi(\mathbf{x}))\Big). \quad (10)$$

The $m_1$ and $m_2$ are termed as the local averages computed as:

$$\begin{aligned} m_1 &= mean\Big(z_0 \in \Big(\{\mathbf{x} \in \Omega \setminus \phi(\mathbf{x}) < 0\} \cap K_\sigma(\mathbf{x})\Big)\Big), \\ m_2 &= mean\Big(z_0 \in \Big(\{\mathbf{x} \in \Omega \setminus \phi(\mathbf{x}) > 0\} \cap K_\sigma(\mathbf{x})\Big)\Big). \end{aligned}$$

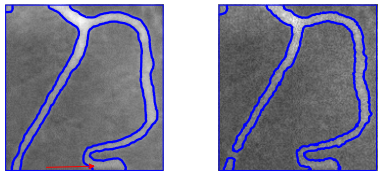

Fig. 1. The performance of LCV model in images with intensity inhomogeneity. Left image: low level additive noise $z_0(\mathbf{x}) + \eta(\mathbf{x})$; Right image: mix of low additive and multiplicative noises $\eta(\mathbf{x})z_0(\mathbf{x}) + \nu(\mathbf{x})$.

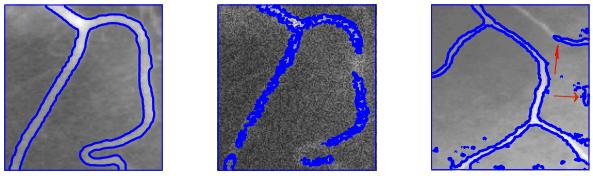

(a) (b) (c)

Fig. 2. The performance of LBF and LIF models. 2a) LBF segmentation results of an image with intensity inhomogeneity without noise; 2b) LBF results of an image with intensity inhomogeneity and in presence of speckle noise with variance $\sigma = 0.05$; 2c) LIF segmentation result for a clean with intensity inhomogeneity image

Keeping $m_1$ and $m_2$ fixed, minimization of the functional in equation (9) with respect to $\phi$ leads to the following evolution equation:

$$\frac{\partial \phi}{\partial t} = \delta_\epsilon(\phi)(m_1 - m_2)(z_0(\mathbf{x}) - z'(\mathbf{x})). \tag{11}$$

The LIF model uses Gaussian smoothing regularization for the level set function. The drawback of the LIF model is an incapability to handle noise as well as false region representations in some cases. Such an example is shown in Fig. 2c.

For segmentation of multiple regions, Vese and Chan extended their work in [1] by employing several level set functions. Their approach relies on the fact that from $m$ level set functions, $2m$ regions can be represented. A two level set (4-phase) formulation, would be the following:

$$\begin{aligned} F_u(c, \Phi) = {} & \nu \int_\Omega |\nabla H(\phi_1)| + \nu \int_\Omega |\nabla H(\phi_2)| \\ & + \int_\Omega (z_0 - c_{11})^2 H(\phi_1) H(\phi_2) d\mathbf{x} \\ & + \int_\Omega (z_0 - c_{10})^2 H(\phi_1)(1 - H(\phi_2)) d\mathbf{x} \\ & + \int_\Omega (z_0 - c_{01})^2 (1 - H(\phi_1)) H(\phi_2) d\mathbf{x} \\ & + \int_\Omega (z_0 - c_{00})^2 (1 - H(\phi_1))(1 - H(\phi_2)), \end{aligned} \tag{12}$$

where $\Phi = (\phi_1, \phi_2)$ and $c = (c_{00}, c_{01}, c_{10}, c_{11})$ is constant vector evaluated as $c_{11} = \frac{\int_\Omega (z_0(\mathbf{x})) H(\phi_1) H(\phi_2) d\mathbf{x}}{\int_\Omega H(\phi_1) H(\phi_2)}$, $c_{10} = \frac{\int_\Omega (z_0(\mathbf{x})) H(\phi_1)(1 - H(\phi_2)) d\mathbf{x}}{\int_\Omega H(\phi_1)(1 - H(\phi_2))}$, $c_{01} = \frac{\int_\Omega (z_0(\mathbf{x}))(1 - H(\phi_1)) H(\phi_2) d\mathbf{x}}{\int_\Omega (1 - H(\phi_1)) H(\phi_2)}$, $c_{00} = \frac{\int_\Omega (z_0(\mathbf{x}))(1 - H(\phi_1))(1 - H(\phi_2)) d\mathbf{x}}{\int_\Omega (1 - H(\phi_1))(1 - H(\phi_2))}$. As the vector $c$ has been evaluated, the reconstructed image function can be written as:

$$\begin{aligned} z(\mathbf{x}) = {} & c_{11} H(\phi_1) H(\phi_2) + c_{10} H(\phi_1)(1 - H(\phi_2) \\ & + c_{01}(1 - H(\phi_1))(H(\phi_2) + c_{00}(1 - H(\phi_1))(1 - H(\phi_2), \end{aligned} \tag{13}$$

minimizing with respect to $c_{i,j}, i, j = 0, 1$ and $\Phi$ and to get the Euler-Lagrange equations with the following PDEs:

$$\begin{aligned} \frac{\partial \phi_1}{\partial t} = {} & \delta_\varepsilon(\phi_1)\{\nu div(\frac{\nabla \phi_2}{|\nabla \phi_2|}) - [((z_0 - c_{11})^2) \\ & - (z_0 - c_{01})^2) H(\phi_1) + (((z_0 - c_{10})^2) - (z_0 - c_{00})^2) H(\phi_1))]\} \\ \frac{\partial \phi_2}{\partial t} = {} & \delta_\varepsilon(\phi_1)\{\nu div(\frac{\nabla \phi_1}{|\nabla \phi_1|}) - [((z_0 - c_{11})^2) \\ & - (z_0 - c_{01})^2) H(\phi_2) + (((z_0 - c_{10})^2) - (z_0 - c_{00})^2) H(\phi_2))]\} \end{aligned}$$

As mentioned above, the hardest task of segmentation is selective segmentation. The problem so far with selective segmentation would be if the objects are near, the intensity difference is small, or the boundaries are hard to distinguish due to inhomogeniety. The work of Rada and Chen [24] introduced a new method which incorporates 1) a distance function from the given geometrical points 2) an adaptive parameter edge detection function to better influence and decrease the functional and 3) an area-based minimization fitting term to enhance the model's reliability. In terms of level set formulation the model is written in the form:

$$\begin{aligned} \min_{\Gamma, c_2} F(\Gamma, c_2) = \min_{\Gamma, c_2} \Big\{ & \mu \int_\Gamma W(\mathbf{x}) d\mathbf{x} + \lambda_1 \int_{in(\Gamma)} |z_0(\mathbf{x}) - c_1|^2 d\mathbf{x} \\ & + \lambda_2 \int_{out(\Gamma)} |z_0(\mathbf{x}) - c_2|^2 d\mathbf{x} \\ & + \nu \Big[ \Big( \int_{in(\Gamma)} d\mathbf{x} - V_1 \Big)^2 + \Big( \int_{out(\Gamma)} d\mathbf{x} - V_2 \Big)^2 \Big] \Big\}, \end{aligned} \tag{14}$$

where $W(\mathbf{x}) = d(\mathbf{x}) g(|\nabla z_0(\mathbf{x})|)|$, with $g(|\nabla z_0(\mathbf{x})|) = \frac{1}{1 + |\nabla z_0(\mathbf{x})|^2}$ an edge detector function which helps to stop the evolving curve on the edges of the objects, $d(\mathbf{x})$ is a distance function, $d(\mathbf{x}) = \text{distance}((\mathbf{x}), \mathcal{A}) = \prod_{i=1}^{n_1} \left( 1 - e^{-\frac{(\mathbf{x} - \mathbf{x}_i^*)^2}{2\tau^2}} \right)$, $\forall (\mathbf{x}) \in \Omega$ and $\mathbf{x}^*$ geometrical points in the set $\mathcal{A} = \{(x_i^*) \in \Omega, \quad 1 \le i \le n_1\} \subset \Omega$, consisting of $n_1$ distinct points near the boundary of the object to be detected, $\lambda_1, \lambda_2, \mu, \nu$ and are empirical weights, $c_1$ is the known mean of the polygon constructed with the given markers (with the supposition that the markers are placed inside the object or not too far the boundaries), $c_2$ is a region term defined below in equation (15), representing the mean intensity outside the target object. The last term (weighted by $\nu$) is apriori term stating thet the volume area of the target object remains close to a reference area $V_i, i = 1, 2$. We compute $V_i, i = 1, 2$ as an area of polygon insade and outside the given markers. Keeping $\phi(x, y)$ fixed and minimizing with respect to the unknown intensity outside the object, one gets the following equations for computing $c_2$:

$$c_2(\phi(\mathbf{x})) = \frac{\int_\Omega z_0(x, y)(1 - H_\epsilon(\phi(\mathbf{x})))d\mathbf{x}}{\int_\Omega (1 - H_\epsilon(\phi(x, y\mathbf{x}} \tag{15}$$

if $\int_\Omega (1 - H_\epsilon(\phi(\mathbf{x})))d\mathbf{x} > 0$ (i.e if the curve is nonempty in $\Omega$). In case $c_1$ is considered as an unknown ( a situation where the markers are placed outside the object) than we update similar to $c_2$ with the formula $c_1(\phi(\mathbf{x})) = \frac{\int_\Omega z_0(\mathbf{x}) H_\epsilon(\phi(\mathbf{x})) d\mathbf{x}}{\int_\Omega H_\epsilon(\phi(\mathbf{x})) d\mathbf{x}}$. Keeping $c_1$ and $c_2$ fixed, we minimize (14) with respect to $\phi(\mathbf{x})$ and get the following Euler-Lagrange equation:

$$\begin{aligned} \delta_\epsilon(\phi) \Big\{ \mu \nabla \cdot \left( W \frac{\nabla \phi}{|\nabla \phi|} \right) - \Big[ \lambda_1 (z_0(\mathbf{x}) - c_1)^2 - \lambda_2 (z_0(\mathbf{x}) - c_2)^2 \Big] \\ - \nu \Big[ \Big( \int_\Omega H(\mathbf{x}) d\mathbf{x} - V_1 \Big) - \Big( \int_\Omega (1 - H(\mathbf{x})) d\mathbf{x} - V_2 \Big) \Big] \Big\} = 0. \end{aligned}$$

## III. Proposed Models

The purpose of the proposed method is to be able to deal with image segmentation in the presence of intensity inhomogeneity and high noise. In order to avoid the noise presence in such images but to preserve the image local and fine features, we benefit from a dual denoising data fidelity term for an efficient segmentation. Moreover, to efficiently handle the fine valuable details, we employ an image local information in our model.

Given an image $z_0(\mathbf{x})$ over a domain $\Omega$ we can consider its statistically locally computed approximated image $z(\mathbf{x})$ as follows:

$$z(\mathbf{x}) = f_1(\mathbf{x}) H_\epsilon(\phi(\mathbf{x})) + f_2(\mathbf{x}) \Big( 1 - H_\epsilon(\phi(\mathbf{x})) \Big), \tag{16}$$

where $f_1(\mathbf{x})$ and $f_2(\mathbf{x})$ are spatially varying averages, given in equation (7), used to preserve image local information. The above representation $z(\mathbf{x})$ for a given image $z_0(\mathbf{x})$ will reflect more local information in comparison with piecewise constant and piece-wise smooth approximations models [9], [18], [31]. However, the drawback of considering noise as local information while $f_1(\mathbf{x})$, $f_2(\mathbf{x})$ has been evaluated must be overcome. In order to distinguish between noise and valuable fine detail, we add a coupled denoising term. This constraint ensures accurate recovery of $z(\mathbf{x})$ in the presence of additive noise, multiplicative noise and a combination of them. Thus, we minimise the following function:

$$\begin{aligned} F^{TP}(\phi) = {} & \mu \int_\Omega |\nabla H_\epsilon(\phi(\mathbf{x}))| d\mathbf{x} + (1 - \lambda) \int_\Omega \Big( z(\mathbf{x}) - z_0(\mathbf{x}) \Big)^2 d\mathbf{x} \\ & + \lambda \int_\Omega \Big( \log z(\mathbf{x}) + \frac{z_0(\mathbf{x})}{z(\mathbf{x})} \Big) d\mathbf{x}. \end{aligned}$$

where $\mu$ and $\lambda$ are given constants such that $\mu > 0$, $0 \le \lambda \le 1$ is a trade of parameter between the two data fitting terms and $\int_\Omega |H_\epsilon(\phi(\mathbf{x}))| d\mathbf{x}$ is regularization term. The combined data fidelity terms can efficiently segment images with additive and speckle noises.

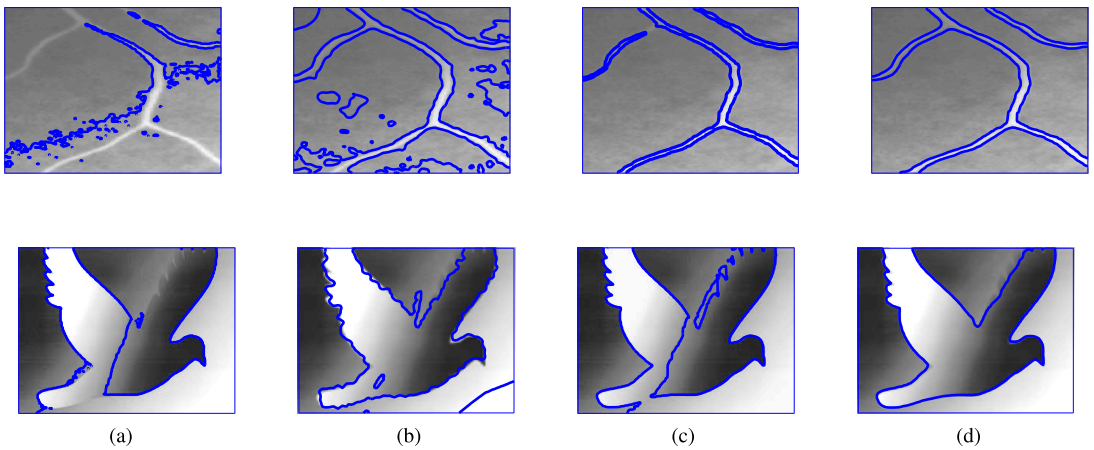

(a) (b) (c) (d)

Fig. 3. Comparison between our model and CVM, LIF and LCV models in segmenting a real blood vessel and the dove images having intensity inhomogeneity. (a) CVM method. (b) LIF method. (c) LCV method. (d) Proposed method.

**Algorithm 1** AOS Method Algorithm for Solving the Two-Phase Level TP Method: $\phi^k \leftarrow TP(\phi^{(k-1)}, \mathcal{A}, \mu, \beta, \epsilon, maxit, tol)$.

Initialize the level set function $\phi(\mathbf{x})$ to be a binary function as follows:

$$\phi^0 = \phi(\mathbf{x}, t=0) = \begin{cases} -\rho & \text{if } \mathbf{x} \in \Omega_0 - \partial\Omega_0 \\ 0 & \text{if } \mathbf{x} \in \partial\Omega_0 \\ \rho & \text{if } \mathbf{x} \in \Omega - \Omega_0 \end{cases}$$

where $\rho > 0$ is a constant, $\Omega_0$ is a subset in the image domain $\Omega$ and $\partial\Omega_0$ is the boundary of $\Omega_0$.
$k = 1$, Compute $f_1(\mathbf{x})$, $f_2(\mathbf{x})$ using Eq. (7)
**for** $iter = 1 : maxit$ **do**
Compute $\phi^{(k)}$ using (29):

$$\phi_i^{(k+1)} \leftarrow \tfrac{1}{2}\sum_{l=1}^{2}(\ I - 2\Delta t A_l(\phi^k))^{-1}\hat{\phi}^{(k)}$$

If $\|\phi^{(k+1)} - \phi^{(k)}\| < tol$ or $iter > maxit$,
set $\phi^{(k)} \leftarrow \phi^{(k+1)}$ Break;
else $\phi^{(k)} \leftarrow \phi^{(k+1)}$
update $f_1(\mathbf{x})$, $f_2(\mathbf{x})$.

**end for**

Minimizing the energy functional $F^{TP}(\phi)$ with respect to $\phi$, we derive the following gradient descent flow:

$$\frac{\partial\phi}{\partial t} = \delta_\epsilon(\phi(\mathbf{x}))\Big[\mu\nabla\cdot\Big(\frac{\nabla\phi(\mathbf{x})}{|\nabla\phi(\mathbf{x})|}\Big) - D\Big(2(1-\lambda)(z(\mathbf{x}) - z_0(\mathbf{x})) + \lambda\frac{z(\mathbf{x}) - z_0(\mathbf{x})}{z(\mathbf{x})^2}\Big)\Big], \quad (17)$$

with Neumann boundary conditions, and $D = (f_1(\mathbf{x}) - f_2(\mathbf{x}))$.

In order to solve equation (17) we use the additive operator splitting (AOS) method as a fast and a low computational cost method. The method has been proposed by Tai *et al.* [20] and Weickert *et al.* [32] and is widely applied. The method decomposes the two-dimensional problem into two one-dimensional ones. After the discretization of equation (17) in a semi-implicit linear system, we develop the iterative approximation scheme, which solves a diagonally dominant tridiagonal linear system as follows: define the

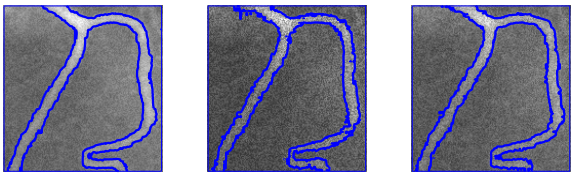

(a) (b) (c)

Fig. 4. The performance of the proposed model in images with intensity inhomogeneity plus a) additive noise, b) multiplicative noise and c) mix of these noises.

AOS solution

$$\phi^{n+1} = \frac{1}{2}\sum_{l=1}^{2}(\ I - 2\Delta t A_l(\phi^n))^{-1}\hat{\phi}^n \quad (18)$$

Here the matrices $A_l, l = 1, 2$, are tridiagonal matrices obtained using central finite differences for the discretisation, detailed in Appendix.

The extension of the proposed model to multiphase vector-valued image segmentation is straightforward.

### *A. Extension of the Proposed Model for Vector-Valued Images*

Since the functional (17) is for gray-scale images, for color/vector-valued images it takes the following form:

$$\begin{aligned} F^{TPV}(\phi(\mathbf{x})) = {} & \mu\int_\Omega \delta_\epsilon(\phi(\mathbf{x}))|\nabla\phi(\mathbf{x})|d\mathbf{x} \\ & + \lambda\int_\Omega \frac{1}{N}\sum_{i=1}^{N}\Big(\log(z_i(\mathbf{x})) + \frac{z_{0,i}(\mathbf{x})}{z_i(\mathbf{x})}\Big)d\mathbf{x} \\ & + (1-\lambda)\int_\Omega \frac{1}{N}\sum_{i=1}^{N}|z_i(\mathbf{x}) - z_{0,i}(\mathbf{x})|^2 d\mathbf{x}, \end{aligned} \quad (19)$$

where $z_{0,i}(\mathbf{x})$ and $z_i(\mathbf{x})$ denotes the $i-th$ frame of given vector-valued image $z_0(\mathbf{x})$ and locally fitted image $z(\mathbf{x})$, respectively. The $z_i(\mathbf{x})$ is computed in the following manner:

$$z_i(\mathbf{x}) = f_{1,i}(\mathbf{x})H_\epsilon(\phi(\mathbf{x})) + f_{2,i}(\mathbf{x})\Big(1 - H_\epsilon(\phi(\mathbf{x}))\Big), \quad (20)$$

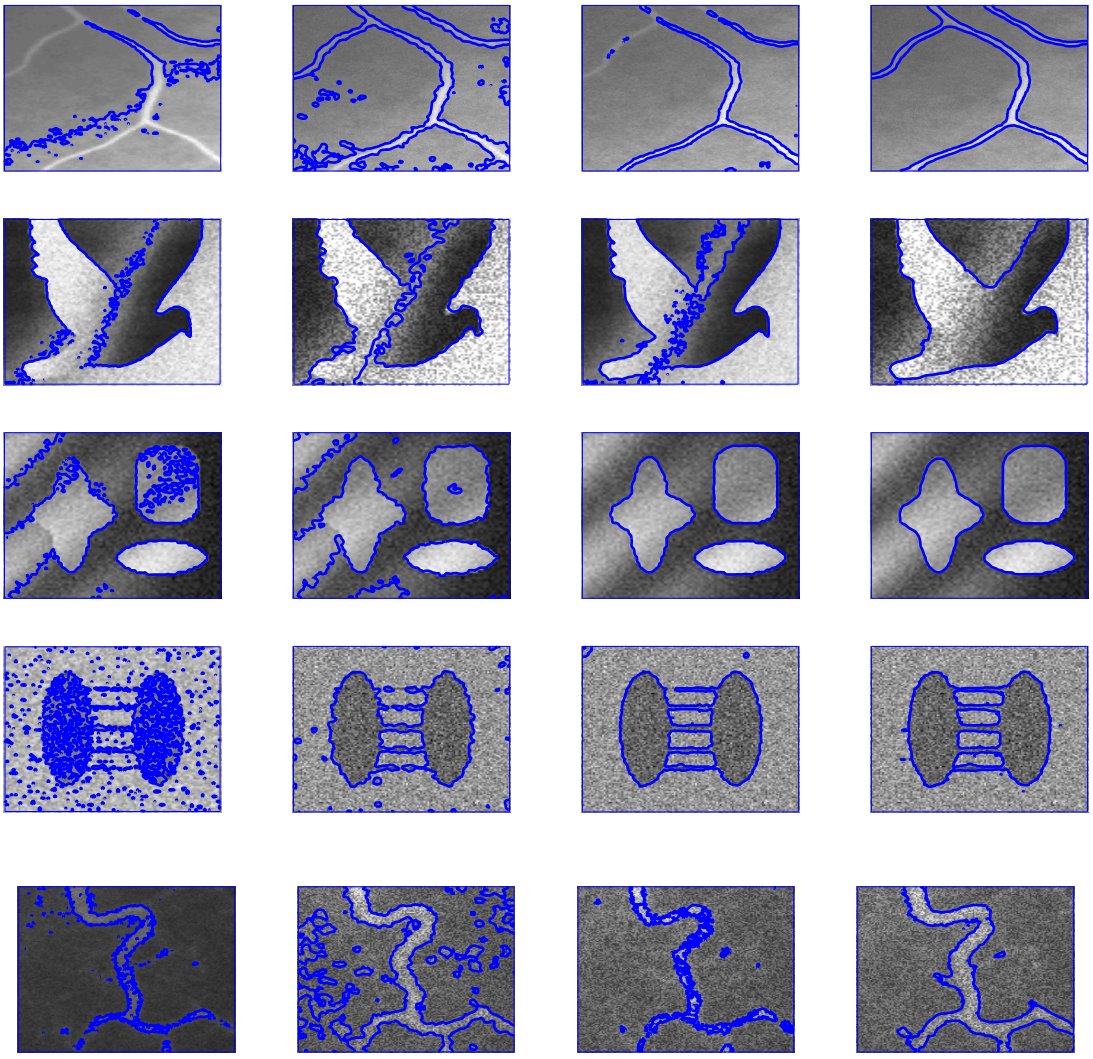

(a) (b) (c) (d)

Fig. 5. Comparison between CVM (first column), LIF (second column) and LCV (third column) models and the proposed model (last column) in segmenting synthetic and real images having intensity inhomogeneity. The image in the first row is affected by additive with variance noise $\sigma = 0.05$, the second row is affected by synthetic noise with $\sigma = 0.05$, whereas the images in the other rows are affected by speckle noise with $\sigma = 0.2$, $\sigma = 0.02$, and $\sigma = 0.05$, respectively. (a) CVM model. (b) LIF model. (c) LCV model. (d) Proposed model.

where $f_{1,i}(\mathbf{x})$ and $f_{2,i}(\mathbf{x})$ are computed in the following manner:

$$f_{1,i}(\mathbf{x}) = \frac{\kappa_\sigma(\mathbf{x}) * H_\varepsilon(\phi(\mathbf{x}))z_{0,i}(\mathbf{x})}{\kappa_\sigma(\mathbf{x}) * H_\varepsilon(\phi(\mathbf{x}))}$$
$$f_{2,i}(\mathbf{x}) = \frac{\kappa_\sigma(\mathbf{x}) * (1 - H_\varepsilon(\phi(\mathbf{x})))z_{0,i}(\mathbf{x})}{\kappa_\sigma(\mathbf{x}) * (1 - H_\varepsilon(\phi(\mathbf{x})))}.$$

Similarly, the equation (17) takes the following form

$$\frac{\partial \phi}{\partial t} = \delta_\epsilon(\phi)\Big[\mu\nabla\cdot\Big(\frac{\nabla\phi(\mathbf{x})}{|\nabla\phi(\mathbf{x})|}\Big) - \frac{1}{N}\sum_{i=1}^{N} D\Big(2(1-\lambda)(z_i(\mathbf{x}) - z_{0,i}(\mathbf{x})) + \lambda\frac{z_i(\mathbf{x}) - z_{0,i}(\mathbf{x})}{z_i^2(\mathbf{x})}\Big)\Big], \tag{21}$$

where $D = (f_{1,i}(\mathbf{x}) - f_{2,i}(\mathbf{x}))$.

### B. Four-Phase Formulation

The proposed model in two-phase level set formulation in equation (17) may not represent each phase in multi-phase images. An example that would represent such a case is the segmentation of a MR brain image, where the regions of gray matter (GM), white matter (WM), and cerebrospinal fluid (CSF) must be distinguished. As the multi-phase level set formulation is useful for some particular phases we will extend the proposed model to a four-phase level set formulation. The multi-phase formulation is straightforward. In the multi-phase level set method, $m$ level set functions can describe $2^m$ regions [1]. In the case of four-phase formulation, two level set functions, $\phi_1$ and $\phi_2$, are evolved such that the given image can be partitioned into four disjoint regions [1]:

$$R_{11} = \{w \in \Omega :\ \phi_1(w) > 0,\ \phi_2(w) > 0\},$$
$$R_{01} = \{w \in \Omega :\ \phi_1(w) > 0,\ \phi_2(w) < 0\},$$
$$R_{10} = \{w \in \Omega :\ \phi_1(w) < 0,\ \phi_2(w) > 0\},$$
$$R_{00} = \{w \in \Omega :\ \phi_1(w) < 0,\ \phi_2(w) < 0\}.$$

Denoting by $M_1 = H_\varepsilon(\phi_1(\mathbf{x}))H_\varepsilon(\phi_2(\mathbf{x}))$, $M_2 = H_\varepsilon(\phi_1(\mathbf{x}))\Big(1 - H_\varepsilon(\phi_2(\mathbf{x}))\Big)$, $M_3 = \Big(1 - H_\varepsilon(\phi_1(\mathbf{x}))\Big)H_\varepsilon(\phi_2(\mathbf{x}))$ and $M_4 = \Big(1 - H_\varepsilon(\phi_1(\mathbf{x}))\Big)\Big(1 - H_\varepsilon(\phi_2(\mathbf{x}))\Big)$, The local averages $f_1(y)$,

(a) (b) (c)

Fig. 6. Performance the vector valued CV and the proposed models in color images. For the proposed model, parameters used are: $\lambda = 0.999$, $\sigma = 10$, $\mu = 0.002$ and $size(z_0) = 156 \times 156$. (a) Initial contour. (b) VVCV result. (c) Proposed method.

$f_2(y)$, $f_3(y)$, $f_4(y)$ are computed in the local interior and local exterior region to fit the image intensities near the point $\mathbf{x}$ in the following way:

$$f_1(\mathbf{x}) = \frac{\kappa_\sigma(\mathbf{x}) * \left[M_1 z_0(\mathbf{x})\right]}{\kappa_\sigma(\mathbf{x}) * M_1}, \quad f_2(\mathbf{x}) = \frac{\kappa_\sigma(\mathbf{x}) * \left[M_2 z_0(\mathbf{x})\right]}{\kappa_\sigma(\mathbf{x}) * M_2},$$
$$f_3(\mathbf{x}) = \frac{\kappa_\sigma(\mathbf{x}) * \left[M_3 z_0(\mathbf{x})\right]}{\kappa_\sigma(\mathbf{x}) * \left[M_3\right]}, \quad f_4(\mathbf{x}) = \frac{\kappa_\sigma(\mathbf{x}) * \left[M_4 z_0(\mathbf{x})\right]}{\kappa_\sigma(\mathbf{x}) * \left[M_4\right]}.$$

Thus, for the four-phase formulation, our locally computed image is given by:

$$z(\mathbf{x}) = f_1(\mathbf{x})M_1(\mathbf{x}) + f_2(\mathbf{x})M_2(\mathbf{x}) + f_3(\mathbf{x})M_3(\mathbf{x}) + f_{4(\mathbf{x})}M_4(\mathbf{x}). \tag{22}$$

We propose the following four-phase (FP) energy, which is an extension of the proposed two-phase energy in equation (17), in the following manner:

$$\begin{aligned} &F^{TPFP}(\phi_1, \phi_2) \\ &= \mu \int_\Omega |\nabla H_\epsilon(\phi_1(\mathbf{x}))| d\mathbf{x} + \mu \int_\Omega |\nabla H_\epsilon(\phi_2(\mathbf{x}))| d\mathbf{x} \\ &\quad + \lambda \int_\Omega \left(\log z(\mathbf{x}) + \frac{z_0(\mathbf{x})}{z(\mathbf{x})}\right) d\mathbf{x} + (1-\lambda) \int_\Omega (z_0(\mathbf{x}) - z(\mathbf{x}))^2 d\mathbf{x}. \end{aligned}$$

The corresponding Euler-Lagrange equations, which drive the active contours represented by the level set functions $\phi_1$ and $\phi_2$, are given by

$$\begin{cases} \dfrac{\partial \phi_1(\mathbf{x})}{\partial t} = \delta_\epsilon(\phi_1(\mathbf{x}))\Big[\mu \nabla \cdot \Big(\dfrac{\nabla \phi_1(\mathbf{x})}{|\nabla \phi_1(\mathbf{x})|}\Big) \\ \quad - D_1\Big(2(1-\lambda)(z(\mathbf{x}) - z_0(\mathbf{x})) + \lambda \dfrac{z(\mathbf{x}) - z_0(\mathbf{x})}{z^2(\mathbf{x})}\Big)\Big], \\ \dfrac{\partial \phi_2(\mathbf{x})}{\partial t} = \delta_\epsilon(\phi_2(\mathbf{x}))\Big[\mu \nabla \cdot \Big(\dfrac{\nabla \phi_2(\mathbf{x})}{|\nabla \phi_2(\mathbf{x})|}\Big) \\ \quad - D_2\Big(2(1-\lambda)(z(\mathbf{x}) - z_0(\mathbf{x})) + \lambda \dfrac{z(\mathbf{x}) - z_0(\mathbf{x})}{z^2(\mathbf{x})}\Big)\Big], \end{cases} \tag{23}$$

where

$$D_1 = \Big((f_1(\mathbf{x}) - f_2(\mathbf{x}) - f_3(\mathbf{x}) + f_4(\mathbf{x}))H(\phi_2(\mathbf{x})) + f_2(\mathbf{x}) - f_4(\mathbf{x})\Big),$$

and

$$D_2 = \Big((f_1(\mathbf{x}) - f_2(\mathbf{x}) - f_3(\mathbf{x}) + f_4(\mathbf{x}))H(\phi_1(\mathbf{x})) + f_3(\mathbf{x}) - f_4(\mathbf{x})\Big).$$

The four-phase segmentation formulation of the proposed model can easily be extended to a multi-phase formulation.

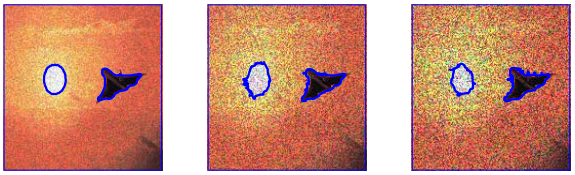

(a) (b) (c)

Fig. 7. Performance of the vector valued CV and the proposed models in color images having different speckle noise level. (a) $\sigma = .02$. (b) $\sigma = .1$. (c) $\sigma = .18$.

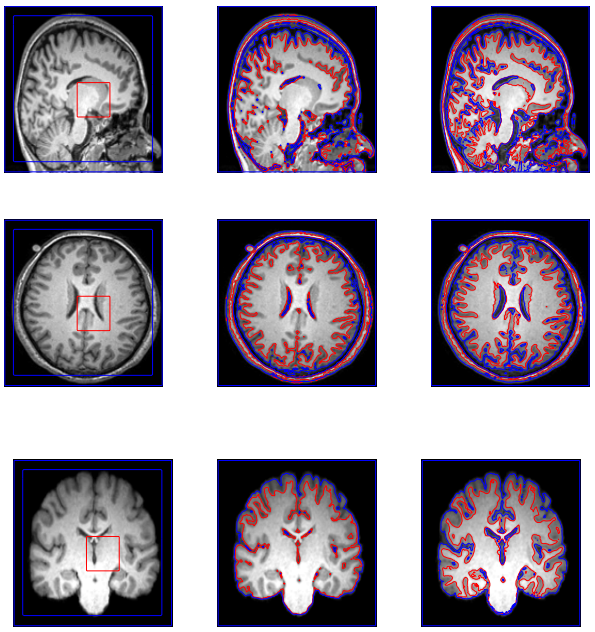

(a) (b) (c)

Fig. 8. Performance of the VC and the proposed models in multi-phase segmenting a real medical brain image. For the proposed model, parameters used are: $\lambda = 0.9995$, $\sigma = 14$, $\mu = 0.1$. (a) Initial contour. (b) VC result. (c) Proposed method.

### C. Selective Segmentation Model for Inhomogeneity Images

To design a variational model reliable for a selective segmentation ensuring same or better performance compared with [24] for images with inhomogeneity we and enrich the equation (14) with a fidelity term:

$$\begin{aligned} &\min_{\Gamma, c_2} F^{STP}(\Gamma, c_2) \\ &= \min_{\Gamma, c_2} \Big\{ \mu \int_\Gamma W(\mathbf{x}) d\mathbf{x} \\ &\quad + \lambda_1 \int_{in(\Gamma)} |z_0(\mathbf{x}) - c_1|^2 d\mathbf{x} + \lambda_2 \int_{out(\Gamma)} |z_0(\mathbf{x}) - c_2|^2 d\mathbf{x} \\ &\quad + \nu\Big[\Big(\int_{in(\Gamma)} d\mathbf{x} - V_1\Big)^2 + \Big(\int_{out(\Gamma)} d\mathbf{x} - V_2\Big)^2\Big]\Big\} \\ &\quad + (1-\lambda) \int_\Omega \Big(z(\mathbf{x}) - z_0(\mathbf{x})\Big)^2 d\mathbf{x} + \lambda \int_\Omega \Big(\log z(\mathbf{x}) + \frac{z_0(\mathbf{x})}{z(\mathbf{x})}\Big) d\mathbf{x}, \end{aligned} \tag{24}$$

Minimizing the energy above energy functional with respect to $\phi$, we get the following gradient descent flow:

$$\begin{aligned} &\delta_\epsilon(\phi)\Big\{\mu \nabla \cdot \Big(W \frac{\nabla \phi}{|\nabla \phi|}\Big) - \Big[\lambda_1 (z_0(\mathbf{x}) - c_1)^2 - \lambda_2 (z_0(\mathbf{x}) - c_2)^2\Big] \\ &\quad - \nu\Big[\Big(\int_\Omega H d\mathbf{x} - V_1\Big) - \Big(\int_\Omega (1-H) d\mathbf{x} - V_2\Big)\Big] \\ &\quad - D\Big(2(1-\lambda)(z(\mathbf{x}) - z_0(\mathbf{x})) + \lambda \frac{z(\mathbf{x}) - z_0(\mathbf{x})}{z(\mathbf{x})^2}\Big)\Big]\Big\} = 0. \end{aligned} \tag{25}$$

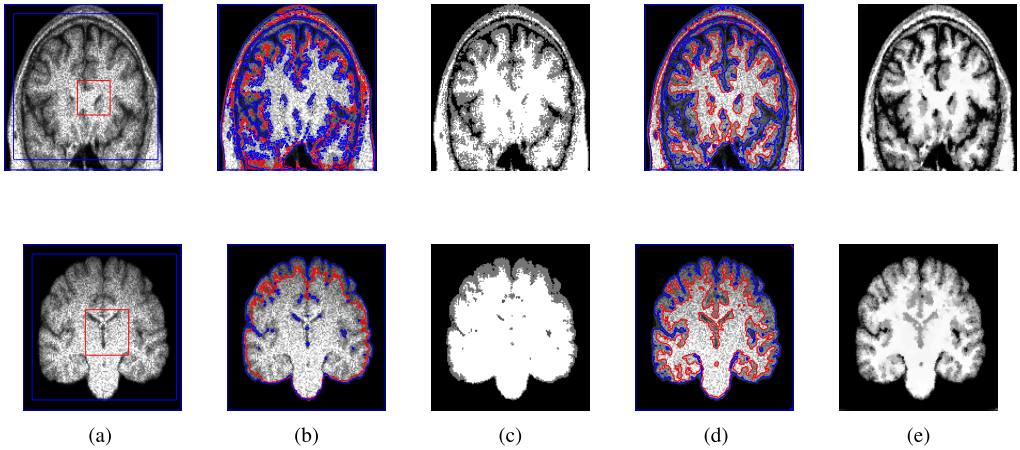

(a) (b) (c) (d) (e)

Fig. 9. Performance of the VC and the proposed models in multi-phase segmenting a real medical brain image having noise and inhomogeneity. For the proposed model, parameters used are: $\lambda = 0.9999$, $\sigma = 14$, $\mu = 0.1$ and $size(z_0) = 150 \times 150$. (a) Initial contour. (b) VC result. (c) Segmented result. (d) Proposed method. (e) Segmented result.

In next section we give some experimental results of our new proposed model compared with some other latest models found in the literature.

## IV. Experimental Results

This section contains test results on real and synthetic images to reveal the performance of the proposed method compared with other competing models in the two-phase segmentation, and in multi-phase segmentation. In addition, the proposed model is also tested in real world color images. For our two-phase model the gray and vector-valued images, we fix $\mu = 0.000005 * imsize$, where $imsize$ is the product of the width and height of the given image sizes, $\lambda = 0.99$, $\Delta t = 1$ and $\sigma = 10$, unless indicated under the figure. To speed up the convergence we can increase the time step $\Delta t$ as the AOS scheme guaranties the stability of the numerical method. To achieve better results the parameters can be tuned depending on the noise level, or alternatively, optimized scheme can be found. We observed from our experiments that the $\lambda$ parameter has to be in the range $0.9 \leq \lambda < 1$ and as the level of noise increases $\lambda$ should be increased by tending to the value of 1. The image size for our experiments varies from $100 \times 100$ to $256 \times 256$ and the code will be provided for research purposes if requested via email. The computation was carried out using MATLAB 7.11.0, in Windows 7 environment on a 2.53GHz Intel Core i3 personal computer with 2GB of RAM.

*Test Set 1: Robustness and Accuracy of the New Model:* In the first test set, we show successful performance of the proposed model in comparison with well known models, such as CVM [33], the LIF model [34], the LCV model [31] for a clean constant intensity image as displayed in Fig. 3. In the first row we consider a vessel MR image with week vessel boundaries and in the second row a synthetic image of a dove where the intensity of foreground decreased gradually from left to right. It can be observed that the (CVM) [33], the LIF model [34], and the LCV model [31] will partially or complicity fail while the proposed method gives satisfactory results. Parameters of comparative methods are chosen such that the results are optimal, for example, the parameters used for the clean dove image, Fig.3 are $\mu = 0.001 * 256^2$, $\alpha = 0.1$, and $\beta = 1$ for the LCV model, $\mu = 1.5$ for the CVM, and $\sigma = 10$ for LIF model. To test the performance of our method in presence of noise, we apply it to images with intensity inhomogeneity together with additive noise (Fig. 4a), multiplicative noise (Fig. 4b) and the mix of these noises (Fig. 4c). In Fig. 4, we demonstrate the ability of the proposed model to perform a correct segmentation these cases.

*Test Set 2: Comparison of the Proposed Model for Images in the Presence of Noise and Inhomogeneity:* We continue the comparison of our model with CVM, LIF and LCV models for images with both intensity inhomogeneity and noise. In the first and the second rows of Fig. 5 we present the satisfactory experimental results using the new model algorithm for capturing a real blood vessel, as well as a synthetic image of a dove with intensity inhomogeneity affected by additive noise and synthetic noise, respectively. In the third, forth and fifth rows of this figure we test images affected with multiplicative noise. The proposed model has efficiently segmented the images, in contrast with the other models considered for comparison which did not perform as well. To show the segmentation accuracy of the proposed model we use the Jaccard similarity coefficient, $J(A, B) = \frac{|A \cap B|}{|A \cup B|}$. Table I shows the results of the mean and the standard deviation of the CVM, the LIF, the LCV models in comparison with the proposed model tested in a set of 10 images. As a general observation, the LCV model produced relatively better results than the CVM and LIF models, but loses local details if the image contains high noise, whereas, the proposed model successfully segments the images by preserving local image details, handling not only severe inhomogeneity but noise as well.

TABLE I

Jaccard Similarity Coefficients for LCV, CVM, LIF and Our Proposed Models

| CVM | LIF | LCV | Proposed method |
|---|---|---|---|
| $0.4 \pm 0.054$ | $0.45 \pm 0.047$ | $0.7 \pm 0.05$ | $0.95 \pm 0.053$ |

*Test Set 3: Comparison of the Proposed Model With a Standard Model in Vector-Valued Images With Intensity Inhomogeneity and Noise:* The proposed model is tested on vector valued images contaminated with speckle noise, as in Figs. 6 and 7, and the results are compared with the classical vector valued Chan-Vese (VVCV) model [1], [9]. These test results show the outstanding performance of the proposed model in segmenting of vector valued images contaminated with different levels of speckle.

*Test Set 4: Comparison of the Proposed Multi-Phase Model With a Standard Model in Images With Intensity Inhomogeneity and Noise:* Fig. 8 shows the performance of the multi-phase version of the proposed method. For convenience, the test results are compared with the VC model [1]. The proposed method performed better in segmenting multi-phase images having intensity inhomogeneity, and furthermore, successfully segmented the given images contaminated with speckle noise and severe inhomogeneity, Fig.9.

*Test Set 5: Comparison of the Proposed New Selective Segmentation Model With Rada-Chen Model [24] for Images With Intensity Inhomogeneity and Noise:* Fig. 10 shows the performance of the proposed selective segmentation model compared with the Rada-Chen model [24]. The first row of this figure shows the comparison results

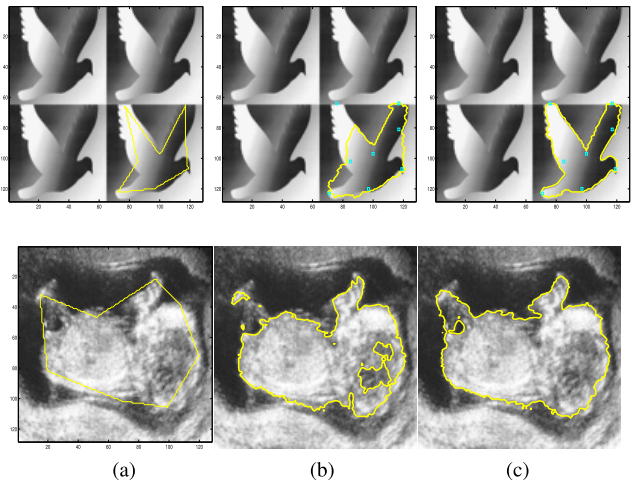

(a) (b) (c)

Fig. 10. Sucesfull segmentation of the new proposed selective segmentation model for a a target dove and the womb in a CT image and its comparison with Rada-Chen model [24].The parameter used are: $\mu = 0.0005 \times imagesize$, $\lambda_1 = \lambda_2 = 1$, $\nu = 0.03$, and $\lambda = 0.9$. (a) Initial contour. (b) Rada and Chen [24] results. (c) New selective model results.

in a synthetic clean image of four doves where the right corner dove has been targeted for segmentation, whereas the second row shows an MR image of a fetus corrupted by noise, severe intensity inhomogeneity and week boundaries. The second column shows the segmentation results obtained by Rada-Chen model [24] and the last column the obtained results by the proposed selective segmentation method. It can be observed that the Rada-Chen model [24] fails to extract the object boundaries as it assumes that the image consists of homogenious region while our model shows the accuracy segmentation of the target object.

## V. Conclusions

We have proposed a new variational global and selective segmentation model suitable for segmenting a range of images that have intensity inhomogeneity, noise and a combination of both. We compared our global segmentation model with previous models, including LCM [33], LIF [34] and LCV [31], and showed that the intensity inhomogeneity degree our model tackles is better than the existing local intensity based models. Through experiments we show that in case of intensity inhomogeneity and noise increasement, the performance of the local intensity based models weakens, whereas, our model produced better results. The reason behind is that we have used double data terms equipped with image local information. This discussion is validated in many figures in our manuscript. To make a successful selective segmentation model capable of dealing with intensity inhomogeneity, we proposed a new model based on 1) a distance function from the given geometrical points 2) an adaptive parameter edge detection function 3) area-based constrain fitting term, and 4) a fidelity term which helps with inhomogeneous and noise. Comparison with existing models shows the correctness of this new selective model for image inhomogeneity. The introduced methods can be widely used in medical images where inhomogeneity and high level of noise have been encountered.

## Appendix
## An Additive Operator Splitting (AOS) Algorithm

We first recalling Eq. (17) in a a two-dimentional domain

$$\frac{\partial \phi}{\partial t} = \mu \delta_\epsilon(\phi) \nabla \cdot \left( \frac{\nabla \phi}{|\nabla \phi|} \right) + \delta_\epsilon(\phi) \left\{ -D \left[ 2(1-\lambda)(z(\mathbf{x}) - z_0(\mathbf{x})) + \lambda \frac{z(\mathbf{x}) - z_0(\mathbf{x})}{z^2(\mathbf{x})} \right] \right\}, \quad (26)$$

where $\mathbf{x} = (x, y)$, $\phi(\mathbf{x}, 0) = \phi^0(\mathbf{x})$ and $\frac{\partial \phi}{\partial \vec{n}}\Big|_{\partial\Omega} = 0$. To avoid singularities we can replace the term $|\nabla \phi|$ with $|\nabla \phi|_\beta = \sqrt{\phi_x^2 + \phi_y^2 + \beta}$, for a small $\beta$. Denoting

$$F(x, y) = \delta_\epsilon(\phi) \left\{ -D \left[ 2(1-\lambda)(z(x, y) - z_0(x, y)) + \lambda \frac{z(x, y) - z_0(x, y)}{z^2(x, y)} \right] \right\}, \quad (27)$$

and $E = \frac{1}{|\nabla \phi|_\beta}$, equations (26) can be written in the compact form:

$$\begin{cases} \frac{\partial \phi}{\partial t} = \mu \delta_\epsilon(\phi) \nabla \cdot (E \nabla \phi) + F(x, y) \\ \quad = \mu \delta_\epsilon(\phi)(\partial_x(E \partial_x \phi) + \partial_y(E \partial_y \phi)) + F(x, y). \end{cases} \quad (28)$$

Discretizing in the spatial step, the equation (26 ) can be rewritten in the matrix-vector form:

$$\frac{\phi^{n+1} - \phi^n}{\Delta t} = \sum_{l=1}^{2} A_l(\phi^n) \phi^{n+1} + F(x, y)$$

where $\Delta t$ is the time step size, $n$ denotes the $n^{th}$ iteration and $A_l$ is the diffusion quantity in the $l$ direction ($l = 1$ and $l = 2$ respectively for $x$ and $y$ direction for the two dimensional case). We can rewrite the above equation in the semi-implicit form:

$$\phi^{n+1} = (I - \Delta t \sum_{l=1}^{2} A_l(\phi^n))^{-1} \hat{\phi}^n \quad \text{for } l = 1, 2$$

and update $\hat{\phi}^n = \phi^n + \Delta t F(x, y)$

By employing the AOS scheme, we split additively

$$\phi^{n+1} = \frac{1}{2} \sum_{l=1}^{2} (I - 2\Delta t A_l(\phi^n))^{-1} \hat{\phi}^n, \quad (29)$$

where the matrices $A_l$, for $l = 1, 2$, are tridiagonal matrices derived using central finite differences:

$$\begin{aligned} &(A_1(\phi^n)\phi^{n+1})_{i,j} \\ &= \mu \delta_\epsilon(\phi^n) \left( \partial_x(E \partial_x \phi^{n+1}) \right)_{i,j} \\ &= \mu \delta_\epsilon(\phi^n) \frac{E^n_{i+1/2,j} (\partial_x \phi^{n+1})_{i+1/2,j} - E^n_{i-1/2,j} (\partial_x \phi^{n+1})_{i-1/2,j}}{h_x} \\ &= \mu \delta_\epsilon(\phi^n) \frac{\frac{E^n_{i+1,j} + E^n_{i,j}}{2} \left( \frac{\phi^{n+1}_{i+1,j} - \phi^{n+1}_{i,j}}{h_x} \right) - \frac{E^n_{i,j} + E^n_{i-1,j}}{2} \left( \frac{\phi^{n+1}_{i,j} - \phi^{n+1}_{i-1,j}}{h_x} \right)}{h_x} \\ &= \mu \delta_\epsilon(\phi^n) \left\{ \frac{E^n_{i+1,j} + E^n_{i,j}}{2h_x^2} (\phi^{n+1}_{i+1,j} - \phi^{n+1}_{i,j}) \right. \\ &\quad \left. - \frac{E^n_{i,j} + E^n_{i-1,j}}{2h_x^2} (\phi^{n+1}_{i,j} - \phi^{n+1}_{i-1,j}) \right\}, \end{aligned}$$

and similarly

$$\begin{aligned} (A_2(\phi^n)\phi^{n+1})_{i,j} &= \mu \delta_\epsilon(\phi^n) \left( \partial_y(E \partial_y \phi^{n+1}) \right)_{i,j} \\ &= \mu \delta_\epsilon(\phi^n) \left\{ \frac{E^n_{i,j+1} + E^n_{i,j}}{2h_y^2} (\phi^{n+1}_{i,j+1} - \phi^{n+1}_{i,j}) \right. \\ &\quad \left. - \frac{E^n_{i,j} + E^n_{i,j-1}}{2h_y^2} (\phi^{n+1}_{i,j} - \phi^{n+1}_{i,j-1}) \right\}. \end{aligned}$$

As $A_l, l = 1, 2$ are tridiagonal matrices allows us to profit from the Thomas algorithm for a fast solution to the system.

## REFERENCES


[1] L. A. Vese and T. F. Chan, "A multiphase level set framework for image segmentation using the Mumford and Shah model," *Int. J. Comput. Vis.*, vol. 50, no. 3, pp. 271–293, Dec. 2002.

[2] F. Akram, J. H. Kim, H. U. Lim, and K. N. Choi, "Segmentation of intensity inhomogeneous brain mr images using active contours," *Comput. Math. Methods Med.*, Jul. 2014, Art. no. 194614. [Online]. Available: https://www.ncbi.nlm.nih.gov/pubmed/25143780

[3] G. Aubert and J.-F. Aujol, "A variational approach to removing multiplicative noise," *SIAM J. Appl. Math.*, vol. 68, no. 4, pp. 925–946, 2008.

[4] V. Badrinarayanan, A. Kendall, and R. Cipolla, "SegNet: A deep convolutional encoder-decoder architecture for image segmentation," *IEEE Trans. Pattern Anal. Mach. Intell.*, vol. 39, no. 12, pp. 2481–2495, Dec. 2017.

[5] N. Badshah and K. Chen, "Image selective segmentation under geometrical constraints using an active contour approach," *Commun. Comput. Phys.*, vol. 7, no. 4, pp. 759–778, 2009.

[6] N. Badshah, K. Chen, H. Ali, and G. Murtaza, "Coefficient of variation based image selective segmentation model using active contours," *East Asian J. Appl. Math.*, vol. 2, pp. 150–169, May 2012.

[7] X. Bresson, S. Esedoḡlu, P. Vandergheynst, J.-P. Thiran, and S. Osher, "Fast global minimization of the active contour/snake model," *J. Math. Imag. Vis.*, vol. 28, no. 2, pp. 151–167, Jun. 2007.

[8] G. J. Brostow, J. Fauqueur, and R. Cipolla, "Semantic object classes in video: A high-definition ground truth database," *Pattern Recognit. Lett.*, vol. 30, no. 2, pp. 88–97, 2009.

[9] T. F. Chan and L. A. Vese, "Active contours without edges," *IEEE Trans. Image Process.*, vol. 10, no. 2, pp. 266–277, Feb. 2001.

[10] L. C. Chen, G. Papandreou, I. Kokkinos, K. Murphy, and A. L. Yuille, "DeepLab: Semantic image segmentation with deep convolutional nets, atrous convolution, and fully connected CRFs," *IEEE Trans. Pattern Anal. Mach. Intell.*, vol. 40, no. 4, pp. 834–848, Apr. 2018.

[11] D. L. Donoho and I. M. Johnstone, "Adapting to unknown smoothness via wavelet shrinkage," *J. Amer. Statist. Assoc.*, vol. 90, no. 432, pp. 1200–1224, 1995.

[12] S. Geman and D. Geman, "Stochastic relaxation, Gibbs distributions, and the Bayesian restoration of images," *IEEE Trans. Pattern Anal. Mach. Intell.*, vol. 6, no. 6, pp. 721–741, Nov. 1984.

[13] L. Grady, "Random walks for image segmentation," *IEEE Trans. Pattern Anal. Mach. Intell.*, vol. 28, no. 11, pp. 1768–1783, Nov. 2006.

[14] C. L. Guyader and C. Gout, "Geodesic active contour under geometrical conditions: Theory and 3D applications," *Numer. Algorithms*, vol. 48, pp. 105–133, Jul. 2008.

[15] J. Chen, T. N. Pappas, A. Mojsilovic, and B. E. Rogowitz, "Adaptive perceptual color-texture image segmentation," *IEEE Trans. Image Process.*, vol. 14, no. 10, pp. 1524–1536, Oct. 2005.

[16] M. Kass, A. Witkin, and D. Terzopoulos, "Active contours models," *Int. J. Comput. Vis.*, vol. 1, no. 4, pp. 321–331, 1988.

[17] L. Zhang, Y. Gao, Y. Xia, K. Lu, J. Shen, and R. Ji, "Representative discovery of structure cues for weakly-supervised image segmentation," *IEEE Trans. Multimedia*, vol. 16, no. 2, pp. 470–479, Feb. 2014.

[18] C. Li, C.-Y. Kao, J. C. Gore, and Z. Ding, "Implicit active contours driven by local binary fitting energy," in *Proc. IEEE Conf. Comput. Vis. Pattern Recognit. (CVPR)*, vol. 42. Jun. 2007, pp. 1–7.

[19] G. Litjens *et al.*, "A survey on deep learning in medical image analysis," *Med. Image Anal.*, vol. 42, pp. 60–88, Dec. 2017.

[20] T. Lu, P. Neittaanmaki, and X. C. Tai, "A parallel splitting-up method for partial differential equations and its applications to Navier-Stokes equations," *RAIRO Math. Model. Numer. Anal.*, vol. 26, no. 6, pp. 673–708, 1992.

[21] T. N. A. Nguyen, J. Cai, J. Zhang, and J. Zheng, "Robust interactive image segmentation using convex active contours," *IEEE Trans. Imag. Process.*, vol. 21, no. 8, pp. 3734–3743, Aug. 2012.

[22] S. Osher and J. A. Sethian, "Fronts propagating with curvature-dependent speed: Algorithms based on Hamilton–Jacobi formulations," *J. Comput. Phys.*, vol. 79, pp. 12–49, Nov. 1988.

[23] L. Rada and K. Chen, "A new variational model with dual level set functions for selective segmentation," *Commun. Comput. Phys.*, vol. 12, no. 1, pp. 261–283, 2012.

[24] L. Rada and K. Chen, "Improved selective segmentation model using one level-set," *J. Algorithms Comput. Technol.*, vol. 7, pp. 509–540, Dec. 2013.

[25] C. Rother, V. Kolmogorov, and A. Blake, "'GrabCut': Interactive foreground extraction using iterated graph cuts," *ACM Trans. Graph.*, vol. 23, no. 3, pp. 309–314, Aug. 2004.

[26] L. I. Rudin, S. Osher, and E. Fatemi, "Nonlinear total variation based noise removal algorithms," *Phys. D, Nonlinear Phenomena*, vol. 60, nos. 1–4, pp. 259–268, 1992.

[27] J. A. Sethian, *Level Set Methods and Fast Marching Methods: Evolvin Interfaces in Computational Geometry, Fluid Mechanics, Computer Vision and Material Science*. Cambridge, U.K.: Cambridge Univ. Press, 1999.

[28] K. Suzuki, "Overview of deep learning in medical imaging," *Radiol. Phys. Technol.*, vol. 10, pp. 257–273, Sep. 2017.

[29] V. Caselles, R. Kimmel, and G. Sapiro, "Geodesic active contours," *Int. J. Comput. Vis.*, vol. 22, no. 1, pp. 61–79, 1997.

[30] W. Yang, J. Cai, J. Zheng, and J. Luo, "User-friendly interactive image segmentation through unified combinatorial user inputs," *IEEE Trans. Image Process.*, vol. 19, no. 9, pp. 2470–2479, Sep. 2010.

[31] X.-F. Wang, D.-S. Huang, and H. Xu, "An efficient local Chan–Vese model for image segmentation," *Pattern Recognit.*, vol. 43, pp. 603–618, Mar. 2010.

[32] J. Weickert, B. M. T. H. Romeny, and M. A. Viergever, "Efficient and reliable schemes for nonlinear diffusion filtering," *IEEE Trans. Image Process.*, vol. 7, no. 3, pp. 398–410, Mar. 1998.

[33] Y. Wu and C. He, "A convex variational level set model for image segmentation," *Signal Process.*, vol. 106, pp. 123–133, Jan. 2015.

[34] K. Zhang, H. Song, and L. Zhang, "Active contours driven by local image fitting energy," *Pattern Recognit.*, vol. 43, no. 4, pp. 1199–1206, Apr. 2010.

[35] F. Zhao and X. Xie, "An overview of interactive medical image segmentation," *Ann. BMVA*, vol. 2013, no. 7, pp. 1–22, 2013.


**Haider Ali** received the M.Sc. degree in mathematics from the University of Peshawar, Pakistan, in 2007, the M.S. degree in applied mathematics (variational models in image processing) from the University of Engineering and Technology Peshawar in 2012, and the Ph.D. degree in applied mathematics (variational models in image processing) from the University of Peshawar in 2016. Since 2010, he has been a Lecturer and Researcher with the University of Peshawar. His research interests include image processing, medical image analysis, robotics, machine learning, segmentation, registration using PDEs, and variational methods.

**Lavdie Rada** received the B.Sc. degree in mathematics from the Faculty of Natural Sciences, Tirana, Albania, the M.Sc. degree in applied mathematics from the Polytechnic University of Tirana, Tirana, and the Ph.D. degree in fast iterative methods for variational models of image segmentation from the Department of Mathematical Sciences, University of Liverpool, Liverpool, U.K. He was a Post-Doctoral Fellow with the Faculty of Engineering and Natural Sciences, Sabanci University, Istanbul, Turkey. Since 2014, she has been a Lecturer with the Engineering and Natural Sciences Faculty, Bahçeşehir University, Istanbul. Her research interests include developing elective solvers for variational image processing models.

**Noor Badshah** received the B.Sc. and M.Sc. degrees in mathematics from the University of Peshawar and the Ph.D. degree in applied mathematics (fast algorithms for image segmentation and variational models) from the Department of Mathematical Sciences, University of Liverpool, Liverpool, U.K. His research interests include fast algorithms for variational image processing models and medical image analysis.